

Rochester Institute of Technology

RIT Digital Institutional Repository

Theses

12-2016

Heart Valve Mathematical Models

Paula Kolar
pjk9030@rit.edu

Follow this and additional works at: <https://repository.rit.edu/theses>

Recommended Citation

Kolar, Paula, "Heart Valve Mathematical Models" (2016). Thesis. Rochester Institute of Technology.
Accessed from

This Thesis is brought to you for free and open access by the RIT Libraries. For more information, please contact repository@rit.edu.

R·I·T

Heart Valve Mathematical Models

by

Paula Kolar

A Thesis Submitted in Partial Fulfillment of the Requirements for
the Degree of
Master of Science in Applied and Computational Mathematics

School of Mathematical Sciences
College of Science

Rochester Institute of Technology
Rochester, NY
December 2016

Committee Approval:

Laura Muñoz
Thesis Advisor

Date

Nathan Cahill
Committee Member

Date

Tamas Wiandt
Committee Member

Date

Matthew J. Hoffman
Director of Graduate Programs, SMS

Date

Abstract

Nearly 100,000 heart valve replacements or repairs are performed in the US every year. Mathematical models of heart valves are used to improve artificial valve design and to guide surgeons performing valve-repairing surgeries. Models can be used to define the geometry of a valve, predict blood flow dynamics, or demonstrate operating mechanisms of the valve.

In this thesis we reviewed features that are typically considered when developing a model of a heart valve. The main modeling methods include representing a heart valve using lumped parameters, finite elements, or isogeometric elements. Examples of a lumped-parameter model and isogeometric analysis are explored. First, we developed a simulation for the lumped-parameter model of Virag and Lulić, and we demonstrated its ability to capture the dynamical behavior of blood pressures, volumes, and flows in the aortic valve region. A Newton-Krylov method was used to estimate periodic solution trajectories, which provide a basis for examining the response to perturbations about initial conditions. Next, an isogeometric model of a heart valve was constructed based on NURBS geometry. The mechanical stiffness of the valve was computed. We discussed how the isogeometric representation could be used in a more complex fluid-structure interaction model to measure surface shear and estimate fatigue failure.

Table of Contents

| | | |
|----|---|----|
| 1 | Statistics of Heart Valve Replacement and Repair | 1 |
| 2 | Uses of Heart Valve Mathematical Models | 1 |
| 3 | Heart Valve Physiology | 1 |
| 4 | Features of a Heart Valve Mathematical Model | 3 |
| | Select Modeling Approach..... | 3 |
| | Capture Complex Geometry or Patient-specific Geometry | 4 |
| | Simplify Symmetric Geometry | 5 |
| | Include Leaflet Thickness | 5 |
| | Arrange Leaflet Fiber Orientation..... | 6 |
| | Refine Model with Fluid-Structure Interaction..... | 6 |
| | Select Material Model..... | 6 |
| 5 | NURBS Primer | 7 |
| 6 | Example Model 1: Lumped Parameter | 9 |
| | Motivation for the Model..... | 9 |
| | Methods..... | 9 |
| | Results..... | 13 |
| 7 | Example Model 2: Isogeometric | 17 |
| | Motivation for the Model..... | 17 |
| | Methods..... | 17 |
| | Results..... | 19 |
| 8 | Discussion | 25 |
| | Lumped Parameter Model..... | 25 |
| | Isogeometric Model | 25 |
| 9 | Conclusions | 26 |
| 10 | Bibliography | 27 |

1 Statistics of Heart Valve Replacement and Repair

Heart valve replacement and heart valve repair are procedures used to remedy complications from congenital and acquired heart valve diseases. According to the *Heart Disease and Stroke Statistics 2016 Update* from the American Heart Association (AHA) [32], 2.5% of the population is affected by valvular heart disease. The 2016 Society of Thoracic Surgeons (STS) *Adult Cardiac Surgery Database* [44] summary reveals that in 2015, over 72,000 valve replacement procedures were performed in the US. These procedures involved the aortic valve (69%), mitral valve (16%), tricuspid valve (14%), and pulmonary valve (less than 1%). Another 12,792 procedures were performed to repair the mitral valve. The database further reveals that the number of procedures has been consistent over the past ten years.

2 Uses of Heart Valve Mathematical Models

Mathematical models of heart valves can be used as a diagnostic tool to provide data on physiological parameters that are difficult to measure. They can be used to produce better artificial valves by predicting changes in dynamic blood flow and valve motion with design changes. Researchers can also easily adjust model parameters and deduce mechanisms that control valvular function. Models have been used to determine the correct size of an implanted bioprosthetic valve. More recent advances in imaging a patient's specific heart valve allow cardiac surgeons to simulate blood flow dynamic outcomes for surgical repairs.

3 Heart Valve Physiology

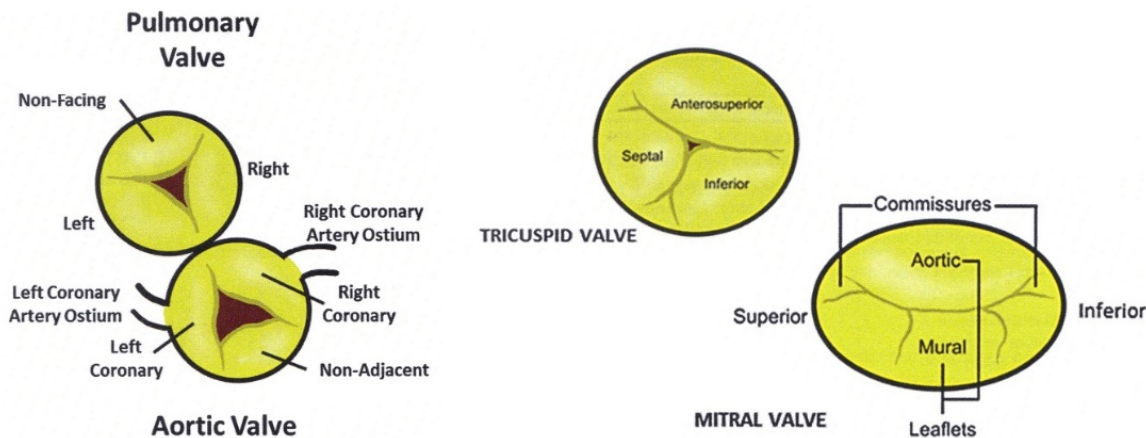
Heart valves regulate the flow of blood from the chambers of the heart. The human heart has four chambers. Circulating blood returning to the heart collects in an atrium and is pumped from the heart by a ventricle. The right atrium and right ventricle transport unoxygenated blood returning from the peripheral circulation to the lungs, and the left atrium and left ventricle transport oxygenated blood returning from the pulmonary system back to the periphery where oxygen is delivered to the cells.

Electrical impulses in the cardiac muscle initiate coordinated contractions of the chamber walls. The blood fluid pressure changes as the chamber contracts or expands. The heart valves open and close in response to pressure gradients that develop across them.

The tricuspid valve separates the right atrium and right ventricle. The mitral valve separates the left atrium and left ventricle. The pulmonary valve releases blood from the right ventricle into the pulmonary artery, and the aortic valve releases blood from the left ventricle into the aorta. Figure 1 shows

each valve and the nomenclature of each leaflet. Generally, the mitral valve has two leaflets with one leaflet having three scalloped edges. Each of other three valves typically has three leaflets. Morphologies vary between people and change with degradation due to age or disease, and the number of leaflets may be ambiguous since the free edge of the leaflets may be irregular in shape forming extra scalloped ridges.

Figure 1: Valve leaflet names using modern attitudinally correct nomenclature (Individual drawings are not to scale)



Heart Valves by Springer US. Reproduced with permission of Springer US in the format Thesis/Dissertation via Copyright Clearance Center.

The two atrioventricular valves, the tricuspid and mitral valves, have common characteristics although the pressure of the circulating blood on the right side of the heart is substantially lower than on the left side of the heart. These valves consist of an annulus, leaflets, and tendinous anchoring cords. The annulus is non-planar, and its shape changes significantly through the cardiac cycle. The annulus forms a base for the valve's leaflets. The leaflets are made of several layers of fibrous tissue. The lamina spongiosa layer carries the mechanical load and has sensory and autonomic nerves that contribute to forming the curvature of the leaflet's arterial side. Papillary muscles within the ventricular wall anchor the leaflets to the heart. Tendinous cords extending from the muscles connect to the leaflet on the ventricular side of the valve. The tendinous cords prevent the leaflets from prolapsing into the atrium. Each cord has an elastic collagen core that supports mechanical load during systole and relaxes into a wavy configuration during diastole. The cords attach to the leaflet along its entire length. The cords that tether the annulus are called the basal cords. Those that attach along the ventricular side of the valve are the strut cords, and the bifurcating cords that attach to the free edge of the leaflet are the fan cords.

Semilunar valve is a common name for a pulmonary or aortic valve. These valves recede into sinuses in the arterial wall as the leaflets open during systole to allow unobstructed blood flow. The valve

closes when the fluid pressure in the ventricles falls lower than the arterial pressure. The valves seal along commissures, which are fibrous areas. Each leaflet has excess tissue along its length beyond the commissures. These free edges are thinner than the commissures and ensure competency of the valve without the tendinous cords tethers like in the atrioventricular valves.

Valves have two failure scenarios. If the valve fails to open fully (i.e., stenosis), the effective orifice area of the valve is reduced. Clinical conditions that cause stenosis are stiffening of the leaflet due to calcification or fusion of commissures. If the valve fails to close (i.e., incompetence of the leaflet contact to seal), blood flow regurgitates back through the valve, making the heart work harder.

Replacement valves are either mechanical or bioprosthetic. Mechanical valves are made from a durable material, and they typically have a ball and cage or a tilted disk configuration. Thrombosis can result from the altered hemodynamics and material biocompatibility issues. Bioprosthetic valves are made of synthetic plastic, treated human or animal tissue, or a homograft from the patient's own tissue. Bioprosthetic valves degrade faster than the original valve, but they operate more naturally and require less anticoagulation therapy than with a mechanical valve [16].

4 Features of a Heart Valve Mathematical Model

The following topics are typically considered when developing a mathematical model of a heart valve.

Select Modeling Approach

The system modeling approach is typically finite element, isogeometric, or lumped parameter. Each has advantages and limitations related to the type of output, required amount of computational resources, and availability in commercial software.

Finite element models partition the object into a network of meshed elements or volumes and allow partial differential equations to be solved across the mesh. This method is widely available in commercial software, and many options are available for static or dynamic analyses. The stress distribution in a static analysis can reveal sites of calcification build-up or of fracture. Halevi [12] modeled an aortic valve with a superimposed image of calcification from a CT scan and predicted the reduction in aortic area due to stiffening of the calcification arrangement. Dynamic analyses animate the valve and show valve dynamics. The boundary conditions for pressure and flow are prescribed, or hemodynamics can be added to model physiologic blood parameters and flow patterns in the circulating blood.

Isogeometric models define geometry with techniques such as Non-uniform rational B-splines (NURBS) and generate a solution on the geometry without using an internal mesh as with finite elements [5]. Modeling biological membranes has been a primary application. Better accuracy can be attained on thin boundary layers between structures and moving fluids such as shear stress at the surface of valves since the solution is analyzed on the exact geometry. The solution can converge with fewer nodes than with finite element analysis [31]. In addition time-consuming mesh generating techniques are not needed, and many mesh-locking difficulties are avoided. The NURBS surface can be refined locally by using T-splines [15][20]. Few commercially-available packages have any isogeometric capability.

Lumped parameter systems simplify the analysis of complex systems by combining effects of subsystems and then applying physics-based relationships between the subsystems. This model requires the least computational resources because it is typically less complex than finite element and isogeometric models. The valve opening and closing dynamics is prescribed by the position of the leaflets (e.g., angle or volume swept by the leaflets.) Virag [39] developed a model that considered the ventricle, aortic valve, aorta, and periphery and produced hemodynamic results near an aortic valve. The pressure waveform showed physiologically correct features such as a dicrotic notch. Aboelkassem [1] expanded the model to include vortices in sinuses. Korakianitis [21] modeled the full circulatory system including all four heart valves and included the ability to consider hemodynamics and valve dynamics with aortic stenosis and aortic regurgitation. The lumped parameter system can also be used to define pressure and flow boundary conditions for finite element or isogeometric models. Le [24] studied a finite element model of a bi-leaflet aortic prosthetic valve driven by a lumped parameter model of the left ventricle.

Capture Complex Geometry or Patient-specific Geometry

Imaging data can isolate patient-specific geometry, capturing its inherent irregularities and pathologies. Morganti [31] compiled data from CT images of the sinuses and from ultrasound images of the leaflet free edge and constructed a patient-specific valve by fitting a NURBS with a least square fitting technique. However, accurate modeling is limited by obtaining accurate dimensions. The valve experiences dimensional changes over the cardiac cycle [37]. The sinus diameter has the most significant change. The diameter at the ventricular outlet does not vary significantly, but the diameter of the aortic root changes. The height of the valve from attachment at the aortic root to top of commissure attachment does not vary. The length of the free edge increases slightly with pressure, and the coapt length, which is the length closed leaflets are in contact in the radial direction, decreases with pressure. The leaflet thickness thins.

Several geometric models of heart valves have been pursued to identify and quantify dimensions needed to develop simplified models. These models are typically defined by a few parameters. Haj-Ali

[11] determined parametric equations to represent a 3D model of a closed tri-leaflet aortic valve with sinuses. The model is scalable by the aortic root diameter, and its shape can be varied by fitting in vivo imaging data points to shaping parameters in the equations. Labrosse [23] determined the relationship between five dimensional parameters to produce a properly-sealing aortic valve. The model suggests dimensional guidelines for valve replacement and repair, and it also provides criteria for bounds on finite element input parameters to create a physiologic-shaped valve that does not prolapse.

The attachment at the aortic root has been assumed to be an ellipse [37], parabola [29], or circle [11][37]. A detailed study of the line of attachment by Grousseau [10] concluded that the curves are non-planar with an elliptical axial-projection and a parabolic transverse-projection. Also the leaflet attachments are asymmetric. The right coronary leaflet is the flattest, and the left coronary leaflet has the most curvature.

The load-bearing surface has been assumed to be cylindrical [37] [23]. The dimensions were assumed to be fixed through the cardiac cycle, and the plane at the aortic diameter and the plane at the commissure diameter were assumed to be parallel. The cylindrical surface of the open leaflet flips around the commissure attachment line plane, and a reflected cylindrical surface is formed to support the load. Ma [26] concluded that the aortic leaflet of the mitral valve was convex to the left ventricle near the annulus and concave near the free edge. The surface was also assumed to be a semi-paraboloid in another study [29].

Simplify Symmetric Geometry

In most models leaflet symmetry is assumed, and only one leaflet or one-half of the leaflet is modeled to reduce computation time. Models that consider hemodynamic differences when the valves do not coapt centrally need to include at least two adjacent leaflets [34]. One leaflet can close faster if an asymmetric retrograde blood flow is directed towards it [24]. Asymmetric vortices contributed to higher flow shear stress on the leaflets of asymmetric bicuspid aortic valves, a congenital disorder known to have a high incidence of stenosis due to calcification [28]. Modeling patient-specific valves from imaging data are inherently asymmetric and need to include all leaflets.

Include Leaflet Thickness

The leaflet can be modeled as a 2D shell or 3D object with a small thickness. Most models use a simplified shell with a Kirchhoff–Love method where the thickness remains normal to the 2D plate surface as it deforms. Ma [26] modeled a mitral valve and found that the simulated valve motion matched MRI data better when the mural and aortic leaflets were given different thicknesses.

Arrange Leaflet Fiber Orientation

Fibers are important load-bearing structures within the leaflets. The fibers are arranged non-uniformly, but stained samples show a tendency to align slanted downward toward the leaflet's mid-line on both sides of the leaflet, especially on areas closer to the free edge. As the fibers stretch to support load on the closed valve, the fibers become parallel to the free edge. A finite element simulation performed by Hammer [13] comparing the slanted fibers to a simplified model of circumferential fibers showed a 40% increase in the centrally coapted length. This was due to a greater curvature near the coapted surface and tissue compression towards the leaflet's mid-line.

Refine Model with Fluid-Structure Interaction

Fluid-structure interaction models couple fluid hemodynamics to structural stress. The model considers the elasticity and transverse stretching of the blood vessels and sinuses as the blood flow pulsates. A more accurate stress distribution across the leaflet is determined when hemodynamics that include vortices behind the leaflets [42] and turbulent flow are added to the model.

One of two solvers are typically used to solve fluid-structure interaction problems with heart valves. The immersed boundary method (IB), developed by Peskin in 1972, superimposes an elastic curve (referred to as a fiber) over a fixed mesh where fluid flows through an Eulerian reference frame. Navier-Stokes equations govern the fluid equations, and a traction force is applied to the curve to simulate the shear force transmitted by the fluid. The Arbitrary Lagrangian-Eulerian method (ALE) uses a Lagrangian reference frame for the solid structure and an Eulerian reference frame for the fluid. Computations are performed after mapping both constituents into a third reference frame where the surface has a no-slip condition with equal velocities. In finite element programs this technique requires a deformable mesh or updating of the mesh at each time step. Most heart valve models are based on IB. ALE has been used to model the blood vessels [43] and venous valves [4]. A comparison of IB and ALE for modeling heart valves concluded that the ALE approach was infeasible due to its inability to handle large mesh displacements [2].

Select Material Model

The material model governs how the material deforms from applied loads. Most models use a hyperelastic constituent model, which defines a nonlinear relationship between stress (a measure of amount of applied force per area) to strain (a measure of deformation of the material or stretching) based on a strain energy density. The modulus of elasticity of the leaflet is non-linear due to the circumferential wavy tendon fibers that initially unravel when stretched [37]. There are several hyperelastic models. St. Venant–Kirchhoff model is an isotropic hyperelastic model. For anisotropic models mechanical

properties differ in the leaflet's three principal directions. Mooney-Rivlin, May, Newman-Yin, and Gasser-Ogden-Holzappel are anisotropic models. Tepole [38] evaluated the effect of including anisotropy in the material model of an inflated isogeometric-modeled membrane with fixed edges, and he found better agreement with experimental results of physical models than with an isotropic model. Saleeb [34] found more accurate valve motion with an anisotropic model.

5 NURBS Primer

Non-uniform rational B-splines (NURBS) form a mathematical representation of a shape [5][8][33]. The shape can be a curve, surface, volume, or higher-dimensional solid. NURBS are composed of rational B-splines and are defined by de Boor control points, their weights and a set of basis functions. NURBS equations are given in Equations (1)-(4) below. NURBS are useful because they form exact conical shapes as well as free form shapes. The NURBS derivatives are easily calculated and can be easily manipulated, which makes it easy to create continuous smooth surfaces and to seamlessly combine NURBS patches together. More elaborate shapes can also be formed by revolving or sweeping a NURBS (e.g., creating a surface from a swept or revolved NURBS curve).

$$N_{i,0}(\xi) = \begin{cases} 1 & \text{if } \xi_i \leq \xi < \xi_{i+1} \\ 0 & \text{otherwise} \end{cases} \quad (1)$$

$$N_{i,p}(\xi) = \frac{\xi - \xi_i}{\xi_{i+p} - \xi_i} N_{i,p-1}(\xi) + \frac{\xi_{i+p+1} - \xi}{\xi_{i+p+1} - \xi_{i+1}} N_{i+1,p-1}(\xi) \quad (2)$$

$$R_{(i)}^p(\xi) = \frac{N_{i,p}(\xi) w_i}{\sum_{i=1}^n N_{i,p}(\xi) w_i} \quad (3a)$$

$$C_{(\xi)} = \sum_{i=1}^n R_{(i)}^p(\xi) P_i \quad (3b)$$

$$R_{(i,j,k)}^{p,q,r}(\xi, \eta, \varphi) = \frac{N_{i,p}(\xi) M_{j,q}(\eta) L_{k,r}(\varphi) w_{i,j,k}}{\sum_{i=1}^n \sum_{j=1}^m \sum_{k=1}^l N_{i,p}(\xi) M_{j,q}(\eta) L_{k,r}(\varphi) w_{i,j,k}} \quad (4a)$$

$$V_{(\xi,\eta,\varphi)} = \sum_{i=1}^n \sum_{j=1}^m \sum_{k=1}^l R_{(i,j,k)}^{p,q,r}(\xi, \eta, \varphi) P_{i,j,k} \quad (4b)$$

$i [j, k]$: knot vector index in parametric $\xi [\eta, \varphi]$ dimension from 1 to $n + p + 1$ [$m + q + 1, l + r + 1$]

$p [q, r]$: series from 1 to order of basis function

$\xi_i [\eta_j, \varphi_k]$: knot element in parametric $\xi [\eta, \varphi]$ dimension

ξ $[\eta, \varphi]$: coordinate along parametric ξ $[\eta, \varphi]$ dimension

$N[M, L]$: basis function along parametric ξ $[\eta, \varphi]$ dimension

n $[m, l]$: number of basis functions in parametric ξ $[\eta, \varphi]$ dimension

P_i or $P_{i,j,k}$: 3D control point that corresponds to NURBS coordinate in subscript

$w_{(i)}$ or $w_{(i,j,k)}$: control point weights for each NURBS coordinate in subscript

$C(\xi)$: curve coordinates in physical space as a function of parametric coordinates

$R_{(i)}^p(\xi)$: rational basis function

$R_{(i,j,k)}^{p,q,r}(\xi, \eta, \varphi)$: shape function of tri-variate NURBS

$V_{(\xi,\eta,\varphi)}$: volumetric coordinates in physical space as a function of parametric coordinates

Each point on the NURBS is a weighted linear combination of the control point coordinates. The dimension of the control point coordinates determines the dimension of the space where the NURBS resides. For instance, if a NURBS curve is determined by a set of control points with three coordinates, the curve lies in three dimensional space. A property of NURBS is that its shape is bounded by a polygon formed by the control points. The bounding polygon is called a convex hull for 2D and a control mesh for 3D. A similar NURBS property is the variation diminishing property, which exists for NURBS curves but is not scalable to higher dimensions, and hence the property is not seen in NURBS surfaces or NURBS volumes. The variation diminishing property states that a plane intersects a NURBS curve no more times than it intersects its control polygon.

The control point weights determine the affinity of the points on the NURBS to the control points. A higher weight draws the NURBS closer to a control point. Sometimes the weights are interpreted as an additional dimension to the control point coordinates. Pictorially the final NURBS form can be seen as a projection of a B-spline computed with weighted coordinates onto a one degree lower dimension.

NURBS basis functions are defined by the Cox-de Boor recursion formula given in equations (1) and (2). They are generated from two variables: an order (p) and a knot vector sequence (ξ). Higher order basis functions are formed from a linear combination of lower order basis functions.

The order of the basis function determines how many neighboring control points contribute to the support of the bases function. A second-order bases is supported by three adjacent control points. The support is always one greater than the order. Each set of basis functions for a given order conforms to the partition of unity; therefore each basis function is a coefficient in the linear combination to define the

NURBS. The shape of NURBS can be adjusted locally without changing its overall shape due to the basis function properties of local support and partition of unity.

The knot vector is a non-decreasing set of numbers that define how the parametric space is partitioned. The basis functions map this parametric space into physical space. Each dimension of parametric space has a knot vector. Hence, a univariate NURBS curve has one knot vector. A bi-variate NURBS surface has two knot vectors, and a tri-variate NURBS volume has three knot vectors. A knot vector is called open when its initial and final elements have multiplicity equal to one greater than the order of the basis function. Open knots create NURBS whose end or corner points coincide with control points. For bi-variate NURBS or higher, the boundary of the NURBS is a NURBS that has one less dimension (i.e., the boundary of a NURBS surface is a NURBS curve). The total number of knots must be equal to the sum of the control points and order. However, as specified in the NURBS acronym, knot vector elements do not need to be uniformly spaced. Non-uniformity and multiplicity of knots affects how the control point coordinates contribute to the NURBS shape, and the order of the basis function and multiplicity of the knots determine the continuity of the surface and its derivatives at the knots.

NURBS can be refined by increasing the order of the basis function or by adding additional knots. Adding knots increases the number of basis functions but keeps the continuity of NURBS. Order elevation increases the continuity of higher derivatives but has a lower increase in basis functions than with knot insertion. Refinement is done globally and cannot be performed locally on a patch, and refinement is not able to produce a “water-tight” geometry.

6 Example Model 1: Lumped Parameter

Motivation for the Model

We investigated a lumped parameter model and verified that it captures the cyclic behavior of the blood pressure, flow rates, and volumes associated with a portion of the circulatory system that includes the aortic valve and left ventricle. A Newton-Krylov method was used to estimate periodic solution trajectories of the model, which provide a basis for examining the response to perturbations about initial conditions.

Methods

The lumped parameter model is based on the heart valve model by Virag and Lulić [39]. It consists of a chamber for the left ventricle, leaflets with a prescribed opening and closing time delay, a chamber for the arterial system, and peripheral capillary resistance. The variables used in the model are described in Table 1. The leaflet dynamics and leaflet flow function, Q_L , are shown in Table 2. The leaflet

dynamics are modeled as a conic section of varying volume. The flow of the leaflets, Q_L , is a continuous piecewise function that is divided into seven segment over the cardiac cycle. The function passes to consecutive segments as a pressure or leaflet volume criterion is met. The model equations are given in (5)-(12). The left ventricle pressure drives the system and is a linear combination of systolic and diastolic pressure (5), and the coefficients of the linear combination are defined by an interpolation function shown in Figure 2.

$$p_{Lv} = \alpha(t)p_s + (1 - \alpha(t))p_d = \alpha(t)E_{es}(x_1 - V_{0,es}) + (1 - \alpha(t))E_d(x_1 - V_{0,d}) \quad (5)$$

$$p_{sa} = E_{sa}(x_2 - V_{0,sa}) + \eta_{sa}(x_5 - x_4) \quad (6)$$

$$\dot{x}_1 = -x_4 + Q_L(x_3, x_4) \quad (7)$$

$$\dot{x}_2 = x_4 - x_5 \quad (8)$$

$$\dot{x}_3 = Q_L(x_3, x_4) \quad (9)$$

$$\dot{x}_4 = \frac{A_{av}}{\rho L_{av}} \left(p_{Lv} - p_{sa} - \frac{\rho}{2A_{av}^2} x_4^2 \right) \quad (10)$$

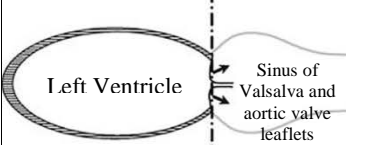
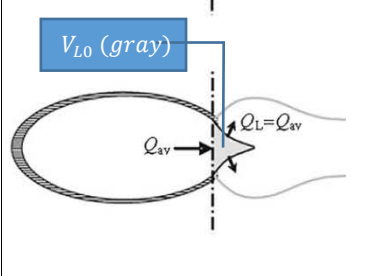
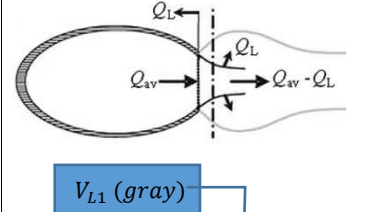
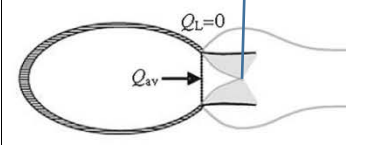
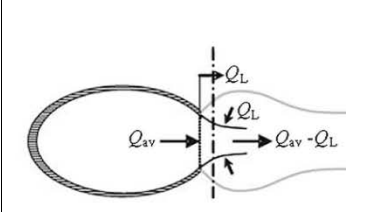
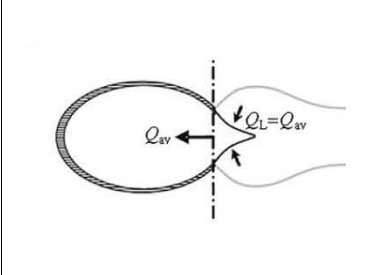
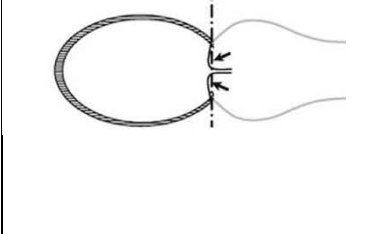
$$\dot{x}_5 = \frac{A_{sa}}{\rho L_{sa}} (p_{sa} - p_{sv} - R_{sc}x_5) \quad (11)$$

$$V_{sa} = \int_0^{t_{hp}} (x_4 - x_5) dt + V_{sa}(0) \quad (12)$$

The set of equations was solved with an operator splitting technique where the pressure variables in equations (5)-(6) were updated between each iteration of solving equations (7)-(11) with a fourth-order Runge-Kutta program. The *nsoli* algorithm by C.T. Kelley was used for the Newton-Krylov method [19]. All code was implemented in Matlab. For initial tests, the parameter values and initial conditions that were suggested in [39] were used.

| Table 1 Virag Heart Valve Model Variables | |
|---|---|
| Patient-specific measured data as measured from a single patient [39] | |
| $A_{av} = 3.46 \text{ cm}^2$ | Area of aortic root |
| $A_{sa} = 1.75 \text{ cm}^2$ | Area of systemic arterial system |
| $T_{hp} = 1062 \text{ msec}$ | Time of a single cardiac cycle |
| $L_{av} = 5 \text{ cm}$ | Effective length between left ventricle pressure and arterial pressure measurement site used in inertia pressure drop estimate |
| $L_{sa} = 90 \text{ cm}$ | Effective length between arterial pressure and systemic venous pressure measurement site used in inertia pressure drop estimate |
| $p_d = 10 \text{ mmHg}$ | Diastolic pressure |
| $p_{sv} = 5 \text{ mmHg}$ | Systemic venous pressure |
| $V_{0,d} = 20 \text{ ml}$ | Equilibrium volume at zero transmural pressure |
| $V_{0,es} = -10 \text{ ml}$ | Unloaded volume at end systole |
| $V_{0,sa} = 300 \text{ ml}$ | Volume of unpressurized arterial system |
| $V_{LV}(\text{ed}) = 124 \text{ ml}$ | Left ventricle volume at end diastole |
| $\text{VTI}=21 \text{ cm}$ | Velocity Time Integral; Stroke Volume= $\text{VTI} * A_{av}$ |
| $\rho = 7.87 \text{e} - 4 \frac{\text{mmHg s}^2}{\text{cm}^2}$ | Density of blood |
| State Variables | |
| $x_1 = V_{lv}$ | Volume of left ventricle; Initial value is $V_{LV}(\text{ed})$ |
| $x_2 = V_{sa}$ | Volume of systemic arterial system; initial value can be calculated from Newton-Krylov method |
| $x_3 = V_L$ | Volume swept by leaflet opening; initial value is 0 |
| $x_4 = Q_{av}$ | Flow through aortic root; initial value is 0 |
| $x_5 = Q_{sc}$ | Flow in systemic capillary system; initial value is calculated from $(E_{sa}(V_{sa}(0) - V_{0,sa}) + \eta_{sa} Q_{av}(0) - p_{sa}(0))/\eta_{sa}$ or can be calculated from Newton-Krylov method |
| Tuned Variables (Tuned to produce v_{max}, T_{acc}, T_{ej} values that matched clinical data) | |
| $E_{es} = 1.7 \text{ mmHg/ml}$ | Ventricular contractility |
| $E_{sa}=0.45 \text{ mmHg/ml}$ | Arterial wall elasticity |
| $\eta_{sa}=.293 \text{ mmHg s/ml}$ | Arterial damping coefficient per volume |
| $R_{sc}=1.429 \text{ mmHg s/ml}$ | Systemic capillary resistance |
| Calculated Input Variables | |
| $E_d = \frac{p_d}{V_{LV}(\text{ed}) - V_{0,d}} = 0.096 \frac{\text{mmHg}}{\text{ml}}$ | Elasticity of left ventricle at end diastole |
| $V_{LV}(\text{es}) = V_{LV}(\text{ed}) - \text{VTI} * A_{av}$ | Left ventricle volume at end systole |
| $p_s = E_{es}(V_{LV}(\text{es}) - V_{0,es})$ | Systolic pressure |
| Calculated Output Variables | |
| $v_{max} = Q_{av}/A_{av}$ | Maximum velocity through aortic root |
| T_{acc} | Time from pressure cross-over ($p_{lv} \geq p_{sa}$) to maximum velocity through aortic root |
| T_{ej} | Time from pressure cross-over ($p_{lv} \geq p_{sa}$) to coaptation of leaflets |

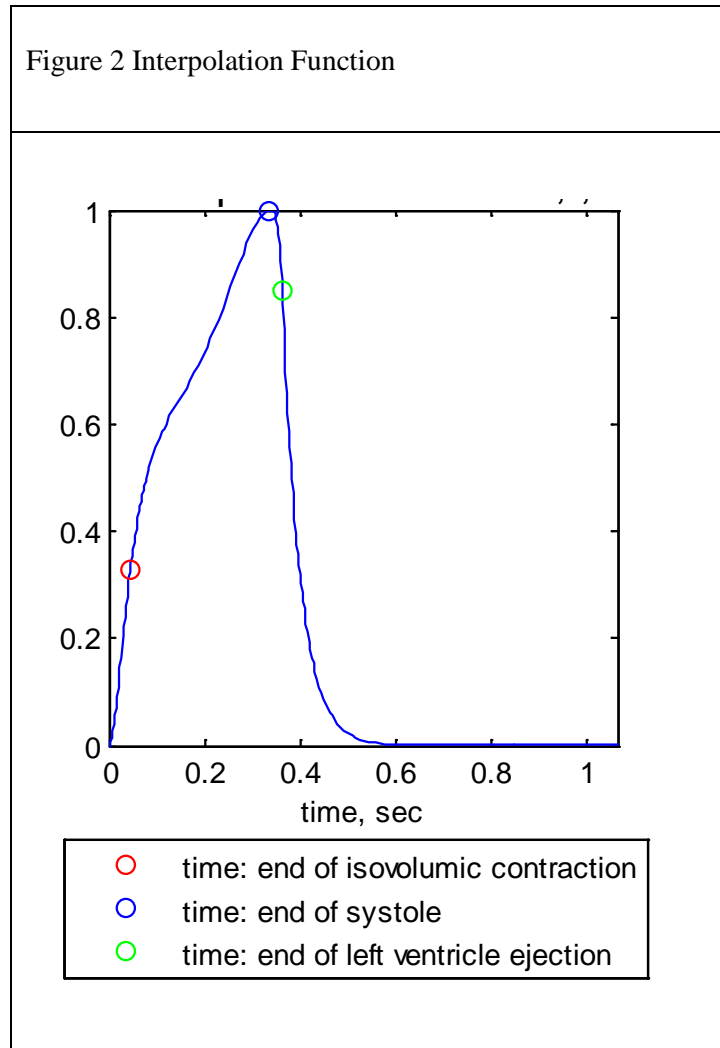
Table 2 Definition of the continuous piecewise function for leaflet flow, Q_L as modeled by Virag [39]

| Graphic from Virag [39] with annotations | Valve progress in cycle | Function $Q_L(V_L, Q_{av})$ |
|---|--|--|
|  | <p>Valve is fully closed; Systole has begun and isovolumetric contraction of heart has started.</p> <p>Advance to next stage when left ventricle pressure exceeds systemic arterial pressure ($p_{lv} \geq p_{sa}$).</p> | <p>0</p> |
|  | <p>Valve is moving but is still sealed; the leaflets sweep out a volume as they open (gray area); Advance to next stage when volume swept by leaflets, V_L, reaches a maximum, V_{L0}, where the coapted surfaces open ($V_L \geq V_{L0}$)</p> <p>V_{L0}: volume swept by leaflet from aortic root to position where seal opens; computed as $\gamma R_{AV}^3 \pi$ where γ is a user-selectable constant (assumed to be 0.3) and R_{AV} is the radius of the aortic valve orifice.</p> | <p>Q_{av}</p> |
|  | <p>Valve is opening;</p> <p>Advance to next stage when valve is fully opened ($V_L \geq V_{L0} + V_{L1}$).</p> <p>$V_{L0} + V_{L1}$: volume swept by leaflet when fully opened; computed as $\beta R_{AV}^3 \pi$ where β is a user-selectable constant (assumed to be 0.6) and R_{AV} is the radius of the aortic valve orifice.</p> | <p>$Q_{av} \left[1 - \left(\frac{V_L - V_{L0}}{V_{L1}} \right)^2 \right]$</p> |
|  | <p>Valve is fully open;</p> <p>Advance to next stage when systemic arterial pressure exceeds left ventricle pressure ($p_{sa} \geq p_{lv}$).</p> | <p>0</p> |
|  | <p>Valve closing;</p> <p>Advance to next stage when volume swept by leaflet, V_L, reaches, V_{L0}, where leaflet coapt.</p> | <p>$Q_{av.co}$: aortic flow when systemic arterial and left ventricle pressures cross ($p_{sa} = p_{lv}$) at the start of this stage</p> <p>$Q_{av} - Q_{av.co} \left(\frac{V_L - V_{L0}}{V_{L1}} \right)^2$</p> |
|  | <p>Valve sealed at coapted surface but leaflets are still moving toward aortic root;</p> <p>Advance to next stage when valve is closed, $V_L = 0$.</p> | <p>$Q_{av.cl}$: aortic flow when the leaflets coapt at the start of this stage.</p> <p>t_{cl}: time when the leaflets coapt.</p> <p>$Q_{av.cl} e^{-(t-t_{cl})Q_{av.cl}/V_{L0}}$</p> |
|  | <p>Valve fully closed and remains closed through diastole.</p> | <p>0</p> |

The values of four parameters (E_{es} , E_{sa} , η_{sa} , R_{sc}) were varied to assess the model's ability to produce calculated values for v_{max} , T_{acc} , and T_{ej} that matched clinical data provided in Virag [39]. Virag "tuned" these values because they are difficult to measure accurately. Each parameter was tested at Virag's suggested value and tested at a higher and lower level for a total of 81 sample test points.

Results

Figure 2 shows the interpolation function that was generated from timing equations provided in [39]. The interpolation function is used to determine the left ventricle pressure that drives the model, and its shape prescribes pressure cross-over timings between the left ventricle and arterial pressures. These two pressure cross-overs cause the leaflets to move and are different from the valve opening and leaflet coaptation times, which are controlled by a time delay built into the model.



The Newton-Krylov method worked well. The values of V_{sa} , V_L , Q_{av} , Q_{sc} , p_{sa} each returned to their initial values at the end of the cardiac cycle. The values for V_{Lv} and p_{Lv} do not need to return to their initial values. The left ventricle is separated from the model during diastole since the aortic valve is closed and the mitral valve is open over this interval. The initial values of V_{Lv} and p_{Lv} are restored at the start of each cycle to re-charge the system as the aortic valve opens. The model runs as a continuous animation of physiologic pressures, volumes, and flows. The system runs over many cycles without introducing any erroneous inflation into the arterial system. See Figure 4-7 for an example of one cardiac cycle. The approximate run time for the Newton-Krylov solver is 65 sec. The solver is only needed once to solve for the initial conditions, then the animation can be run continuously with no delays.

The optimal values of E_{es} and η_{sa} for my coded model were found to be different from the settings suggested by Virag [39]. The combined settings of $E_{es} = 2.2 \text{ mmHg/ml}$, $\eta_{sa} = .193 \text{ mmHg-s/ml}$, $R_{sc} = 1.429 \text{ mmHg-s/ml}$, and any of the three tested levels for E_{sa} generated values of v_{max} , T_{acc} , and T_{ej} (see Table 1 for their definitions) that matched clinical data from Virag [39] better than the Virag's suggested values of $E_{es} = 1.7 \text{ mmHg/ml}$, $E_{sa} = 0.45 \text{ mmHg/ml}$, $\eta_{sa} = .293 \text{ mmHg-s/ml}$, $R_{sc} = 1.429 \text{ mmHg-s/ml}$. The results of comparing calculated ejection and acceleration time and maximum velocity to clinical data is given in Figure 3. The optimal setting points have the same values for E_{es} , η_{sa} , R_{sc} and are the three iterations with a varying value of E_{sa} .

The graphical displays of pressures, volumes, and flows for one animation cycle are shown in Figure 4-7. A simulated dicrotic notch appears on the arterial pressure waveform, and the leaflets show an early slow-closing and late fast-closing that is seen clinically. Both of these simulated clinical attributes are due to the prescribed change in the leaflet flow function at coaptation. Initial values for the optimized settings of $E_{es} = 2.2 \text{ mmHg/ml}$, $E_{sa} = 0.45 \text{ mmHg/ml}$, $\eta_{sa} = .193 \text{ mmHg-s/ml}$, $R_{sc} = 1.429 \text{ mmHg-s/ml}$ are $V_{sa} = 504.376 \text{ ml}$, $Q_{sc} = 52.64001 \text{ ml/s}$, and $p_{sa} = 81.83739 \text{ mmHg}$. The shape of the pressure and volume waveform for these settings has a descending plateau. The roundness and slant of the pressure and flow plateau vary with the settings, mainly with the ventricular contractility and the peripheral resistance settings.

Figure 3 Optimizing Parameters by Matching Verification Data

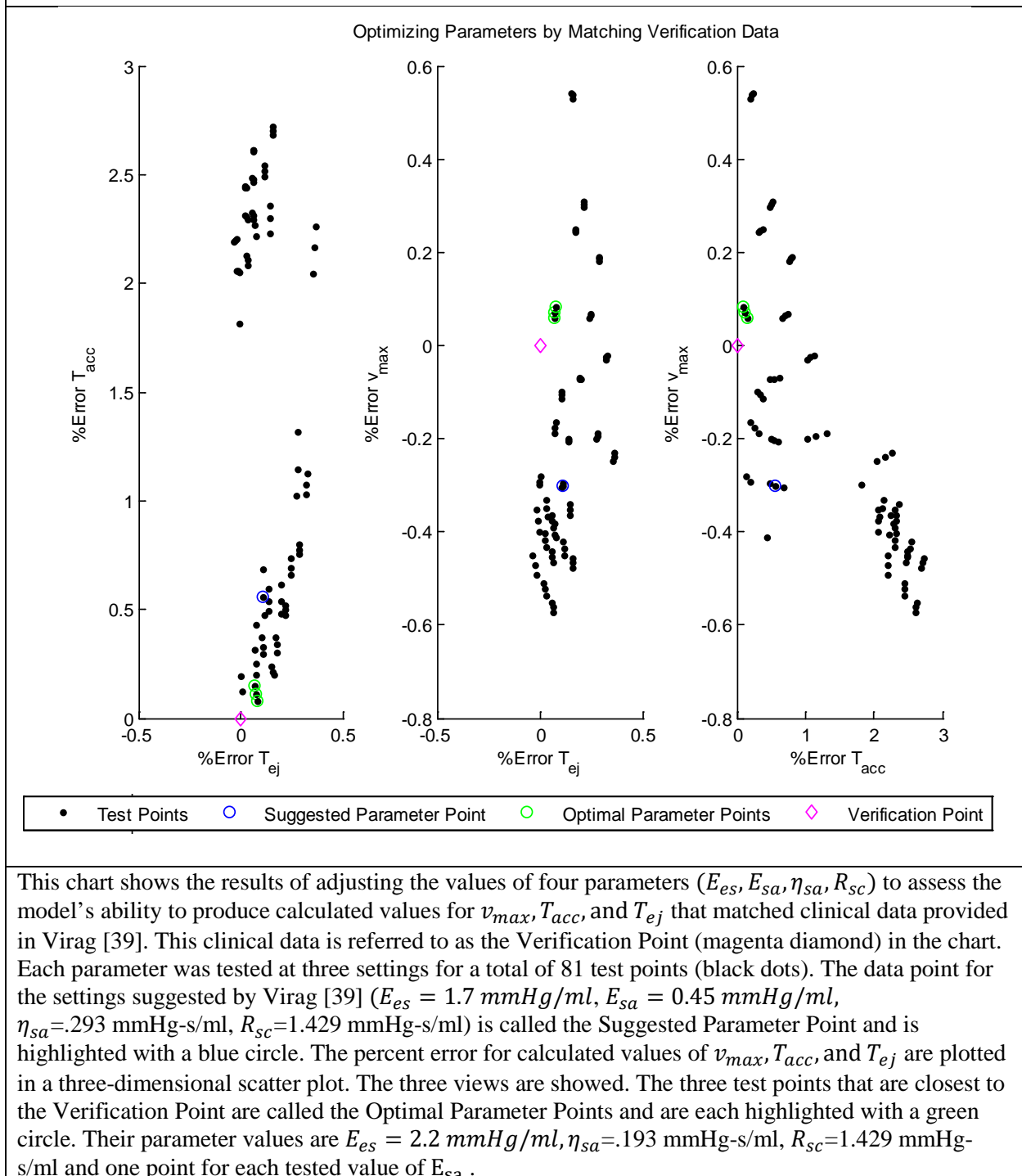
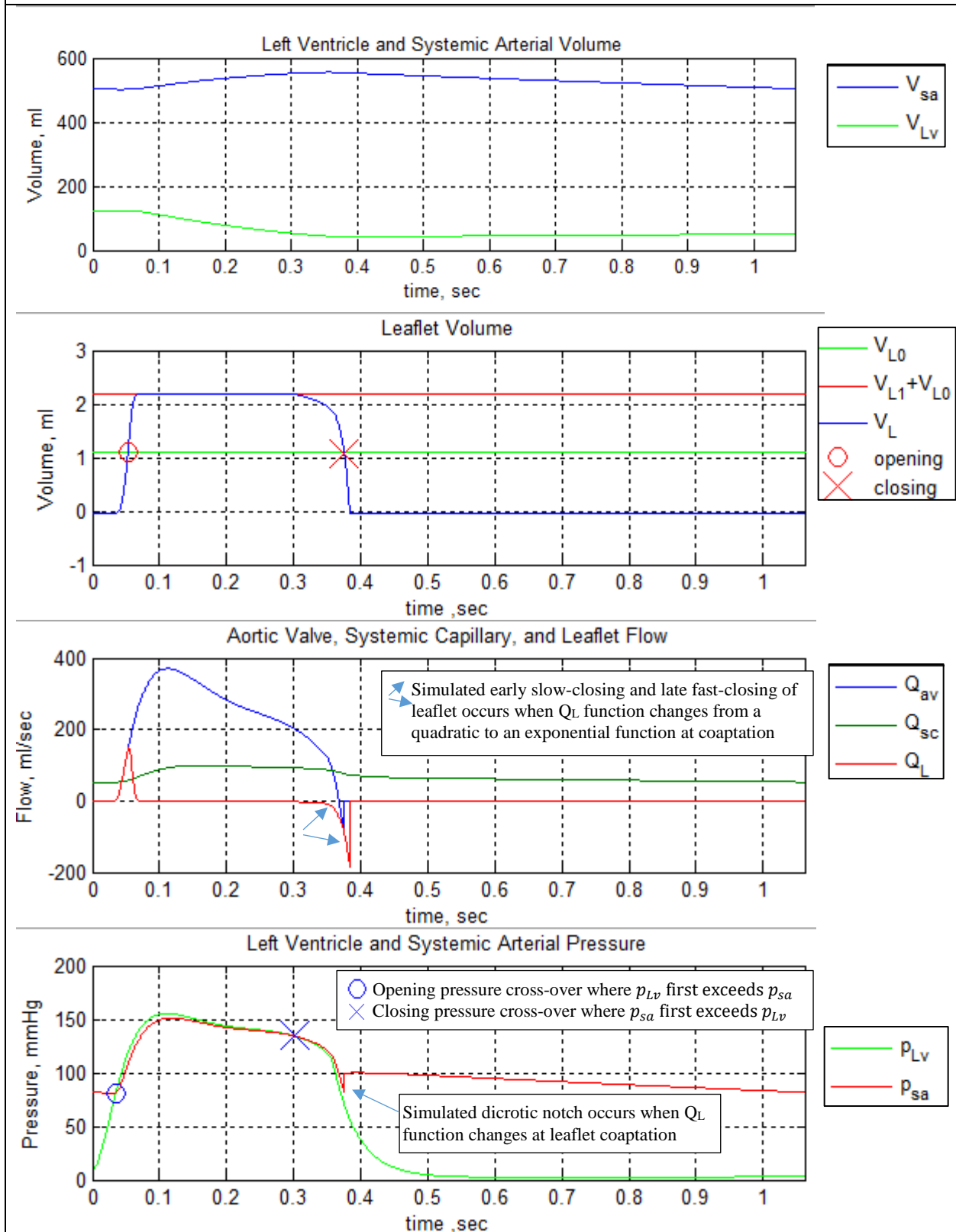


Figure 4 Heart Valve Model with $E_{es} = 2.2 \text{ mmHg/ml}$, $E_{sa} = 0.45 \text{ mmHg/ml}$, $\eta_{sa} = 1.93 \text{ mmHg-s/ml}$, $R_{sc} = 1.429 \text{ mmHg-s/ml}$



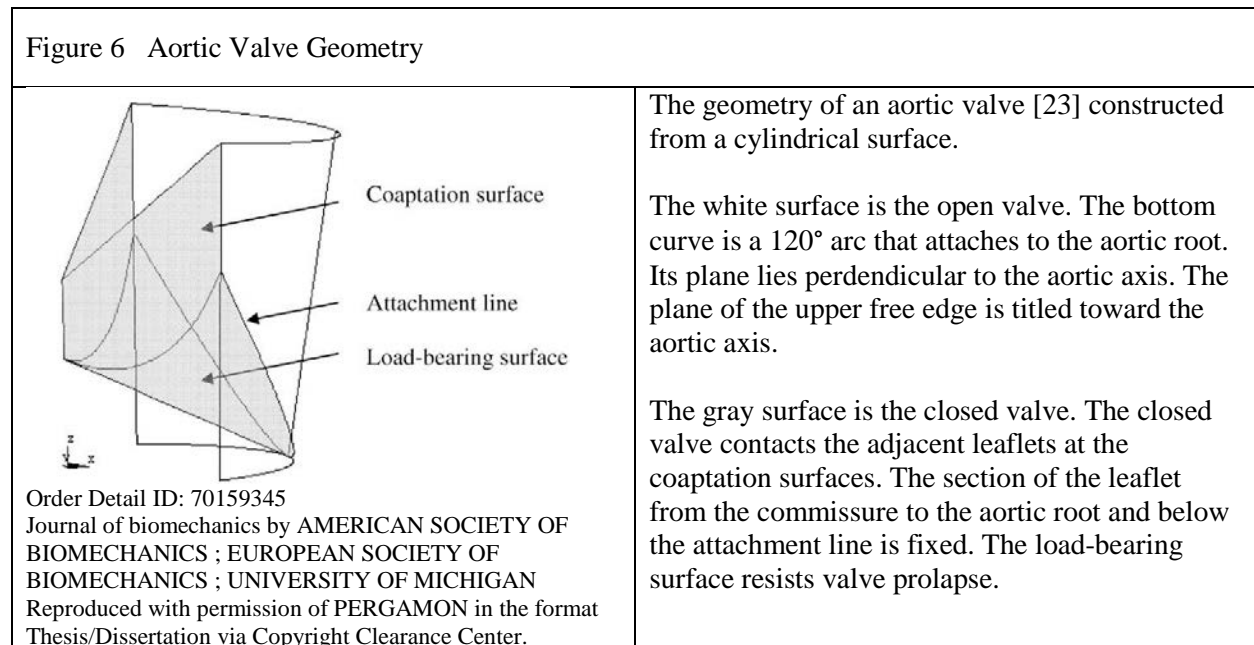
7 Example Model 2: Isogeometric

Motivation for the Model

Shear forces develop on a thin surface layer of solids emerged in a fluid flow. An accurate calculation of shear on the valve surface indicates areas prone to wear and areas prone to stiffening calcification build-up. Isogeometric models provide a better estimate of boundary layer shear than finite element models since isogeometric model solve on the exact geometry of the thin layer. We constructed a valve from NURBS geometry and computed its stiffness. We also produced a routine where it could be used with a FSI model to calculate surface shear or where it could be animated to show the surface contour as it closes.

Methods

We used control points of a hemispherical shell from [5] as test data and used geometry described by Labrosse in [23] to simulate a more realistic cylindrical heart valve. The valve's initial position is an open valve so that the coapted contact surface does not have to be defined but instead can be calculated. The Labrosse geometry is shown in Figure 6. Nominal dimensions for the aortic root diameter (13 mm), commissure diameter (15 mm), and valve thickness (.428 mm) were used. A 12° tilt declination was computed to produce a properly closing valve from equations given in [23].



The valve is generated from a tri-variate NURBS. The xi-direction in parameter space creates NURBS curves along the aortic root and the free edge of the leaflet. Two elements were used to increase

the parameterization, and each curve is second-order. Therefore, its knot vector is [0 0 0 .5 .5 1 1 1]. The eta- and zeta-directions each have a knot vector of [0 0 1 1] with a linear order. The eta-direction generates a ruled surface from the aortic root to the free edge, and the zeta-direction generates a ruled volume through the leaflet's thickness. Control points are coincident with the ends of the curves for both the aortic root and free edge and for the inner and outer layer. These control points have a weight of 1. The intermediate points have a weight of $\sqrt{3}/2$, which is cosine of half the angle of each element's arc [33].

We developed a plotting routine to check the results. The surface points of the volume were computed using equation (4b). Adjacent surface points were connected with the Matlab Delaunay triangulation function and plotted with the *trisurf* function.

Cottrell, Hughes, and Bazilevs [5] developed a process to calculate the stress distribution over a static 3D object simulated as a tri-variate NURBS. They presented code to map the knot vectors in index space into shape functions in parameter space and to calculate the stress on the surface in physical space. They recommend Piegel's code [33] to calculate univariate NURBS basis functions. Shape functions are a summation of univariate NURBS in multiple dimensions. (See NURBS Primer in Section 5 for more information on what NURBS are and how they work). A linear elastic model is assumed where applied force is equal to the stiffness matrix times the displacement vector.

The stiffness matrix for an element within the NURBS is given in equation (13). The local stiffness for each element is combined into a total stiffness for the NURBS shape. We used a Poisson ratio of $\nu = 0.3$, which is in the range for polymers used in artificial valves, and we used a modulus of elasticity of $E = 2$ MPa [14] to estimate an isotropic modulus of elasticity.

The force load of the pulsating flow is both spatially- and time-dependent. Since FSI was not integrated into the model, we used a rough estimate for applied force. The applied force is equal to the mean pressure times the surface area at the aortic root.

We developed a methodology for animating the valve over one cardiac cycle.

$$K^e = \tilde{e}_i \int_{\Omega^e} B_A^T D B_B d\Omega \tilde{e}_j \quad (13)$$

$$D_{ij} = C_{ijkl} = \lambda \delta_{ij} + \mu (\delta_{ik}\delta_{jl} + \delta_{il}\delta_{jk}) \quad (14)$$

$$B_A \vec{e}_i = \begin{bmatrix} \frac{\partial R_A}{\partial x} & 0 & 0 \\ 0 & \frac{\partial R_A}{\partial y} & 0 \\ 0 & 0 & \frac{\partial R_A}{\partial z} \\ 0 & \frac{\partial R_A}{\partial z} & \frac{\partial R_A}{\partial y} \\ \frac{\partial R_A}{\partial z} & 0 & \frac{\partial R_A}{\partial x} \\ \frac{\partial R_A}{\partial y} & \frac{\partial R_A}{\partial x} & 0 \end{bmatrix} \vec{e}_i \quad \text{and} \quad B_B \vec{e}_j = \begin{bmatrix} \frac{\partial R_B}{\partial x} & 0 & 0 \\ 0 & \frac{\partial R_B}{\partial y} & 0 \\ 0 & 0 & \frac{\partial R_B}{\partial z} \\ 0 & \frac{\partial R_B}{\partial z} & \frac{\partial R_B}{\partial y} \\ \frac{\partial R_B}{\partial z} & 0 & \frac{\partial R_B}{\partial x} \\ \frac{\partial R_B}{\partial y} & \frac{\partial R_B}{\partial x} & 0 \end{bmatrix} \vec{e}_j \quad (15)$$

$$|J| = \begin{vmatrix} \frac{\partial x}{\partial \xi} & \frac{\partial x}{\partial \eta} & \frac{\partial x}{\partial \zeta} \\ \frac{\partial y}{\partial \xi} & \frac{\partial y}{\partial \eta} & \frac{\partial y}{\partial \zeta} \\ \frac{\partial z}{\partial \xi} & \frac{\partial z}{\partial \eta} & \frac{\partial z}{\partial \zeta} \end{vmatrix} \quad (16)$$

K^e : Local Stiffness of NURBS element

Ω^e : Domain of an element in parametric space

D, C : Material stiffness matrix with D given in Voigt notation

δ : Kronecker delta

λ, μ : Lamé parameters $\lambda = \frac{E \nu}{(1+\nu)(1-2\nu)}$ and $\mu = \frac{E}{2(1+\nu)}$ where E=modulus of elasticity and ν =Poisson's ratio

A, B : Global shape function numbers

\vec{e}_i, \vec{e}_j : Unit vectors

B : Deformation tensor

R_A, R_B : $= R_{(i,j,k)}^{p,q,r}(\xi, \eta, \varphi)$ from (4a) where the global shape function number A or B correspond to the (i,j,k) coordinates

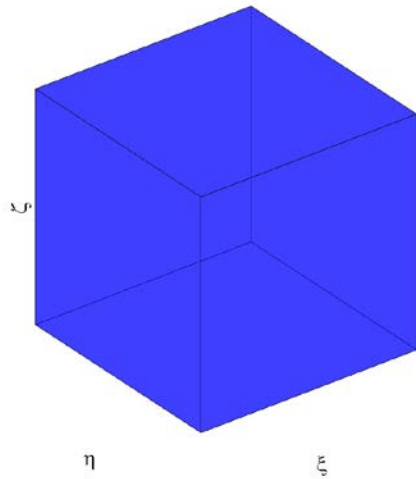
$|J|$: Determinant of the Jacobian that transforms the integral from parametric space into physical space

Results

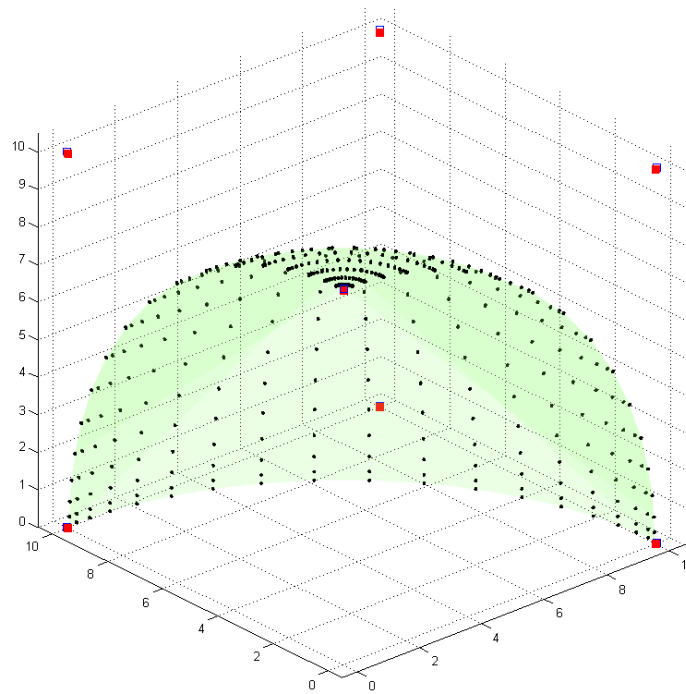
The picture of the test valve is shown in Figure 6. The simulated cylindrical heart valve is shown in Figure 7 and 8. The simulated heart valve is composed of two elements. Since the knot has a multiplicity of two at the interface, the surface only has C^0 continuity at the 0.5 knot.

The code calculates the stiffness matrix by integrating over the entire surface. The code required 3.57 sec per selected quadrature point for the test NURBS and 1.65 sec for the simulated aortic valve.

Figure 6 Test tri-variate NURBS

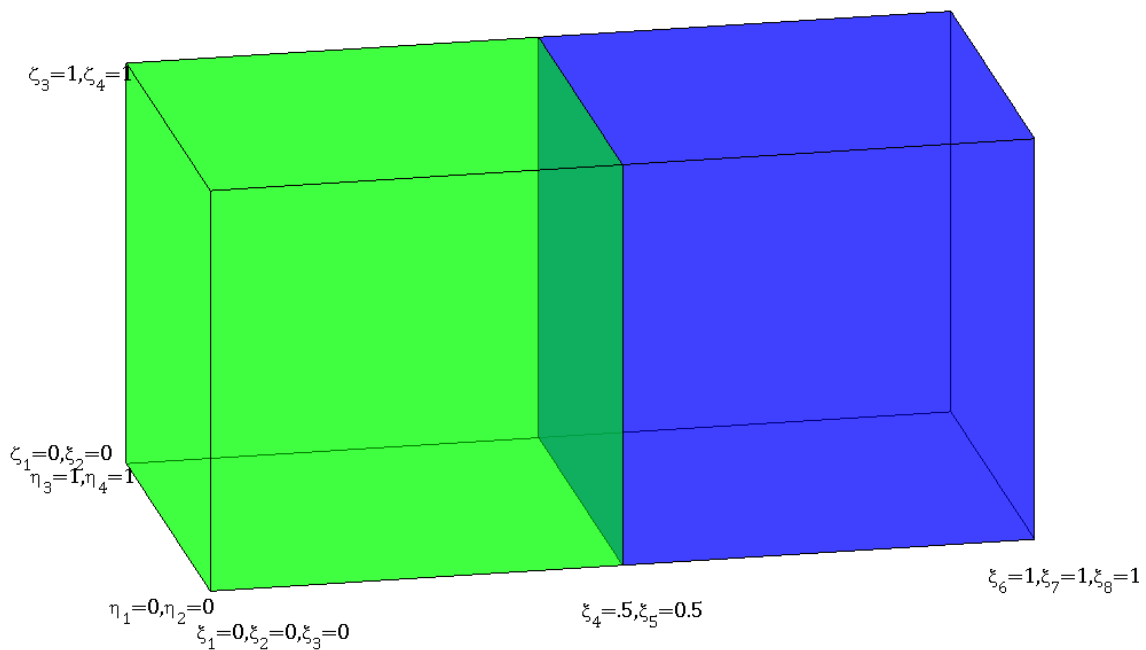
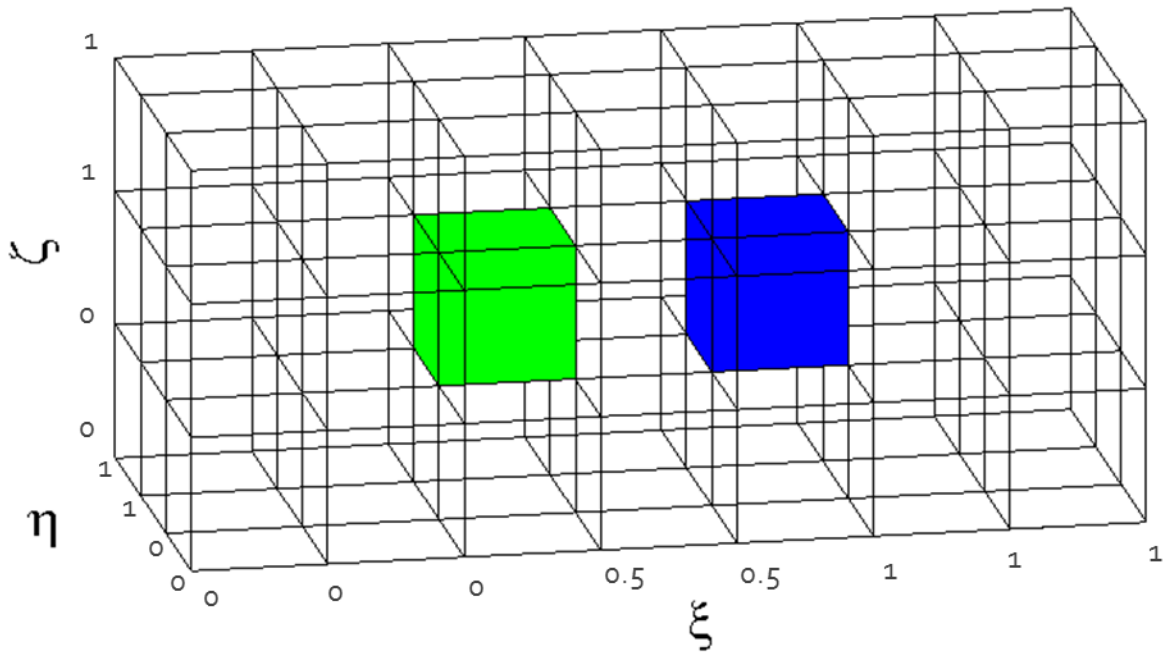


| Control Point Coordinates [5] | Weights |
|-------------------------------|---------|
| (9.98, 0, 0) | 1 |
| (9.98, 9.98, 0) | 0.7071 |
| (0, 9.98, 0) | 1 |
| (9.98, 0, 9.98) | 0.7071 |
| (9.98, 9.98, 9.98) | 0.5 |
| (0, 9.98, 9.98) | 0.7071 |
| (0, 0, 9.98) | 1 |
| (0, 0, 9.98) | 0.7071 |
| (0, 0, 9.98) | 1 |
| (10.02, 0, 0) | 1 |
| (10.02, 10.02, 0) | 0.7071 |
| (0, 10.02, 0) | 1 |
| (10.02, 0, 10.02) | 0.7071 |
| (10.02, 10.02, 10.02) | 0.5 |
| (0, 10.02, 10.02) | 0.7071 |
| (0, 0, 10.02) | 1 |
| (0, 0, 10.02) | 0.7071 |
| (0, 0, 10.02) | 1 |



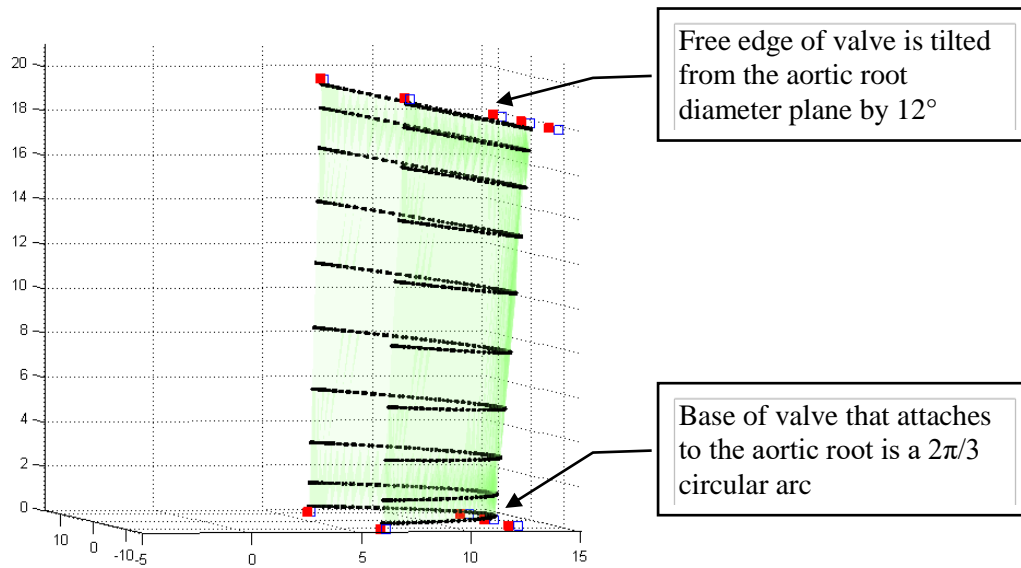
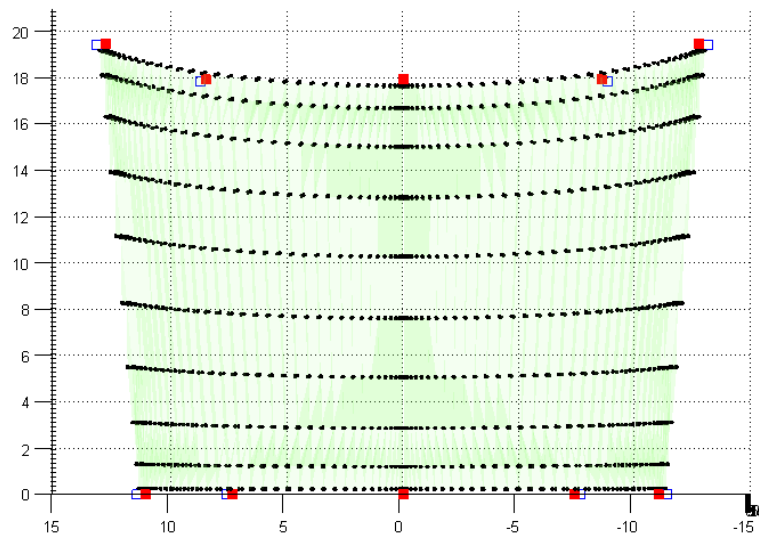
This figure shows the test tri-variate NURBS for the semi-hemispherical shell. The blue cube is the parametric space. The knot values in the ξ -, η -, ζ -direction are $\{0\ 0\ 0\ 1\ 1\ 1\}$, $\{0\ 0\ 1\ 1\}$, $\{0\ 0\ 1\ 1\}$, respectively. The NURBS is composed of a single element formed from 18 control points. The control points were used from [5] and are indicated by red squares and are listed above. Since the shell thickness is small, the control points for the inner and outer layer are overlapping. Three control points are coincident for both the inner and outer shell at the tip as the ξ -direction compresses into a single point at the pole of the sphere in physical space. The quadrature points are indicated by black dots.

Figure 7 Index and parametric space of computed tri-variate NURBS aortic heart valve



This figure shows the index and parametric space of the computed tri-variate NURBS aortic heart valve in the open position. The knot values in the ξ -, η -, ζ -direction are $\{0\ 0\ 0\ .5\ .5\ 1\ 1\ 1\}$, $\{0\ 0\ 1\ 1\}$, $\{0\ 0\ 1\ 1\}$, respectively. The ξ -direction has a repeated knot between the two elements.

Figure 8 Computed tri-variate NURBS aortic heart valve in the open position



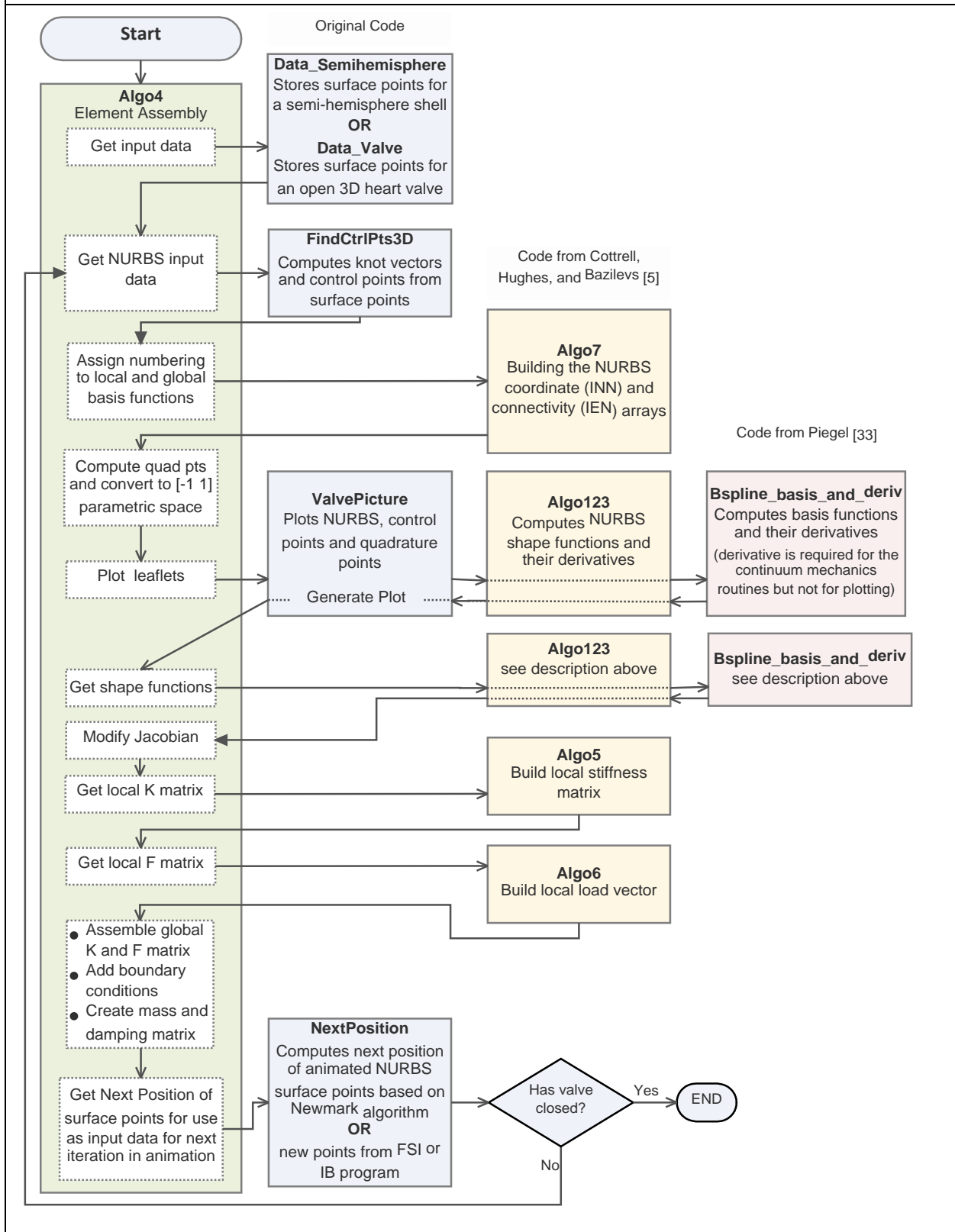
This figure shows two views of the same tri-variate NURBS aortic heart valve in the open position. The upper view shows the ventricle-facing side of the valve. The lower view shows a side-view of the valve. The NURBS is computed from 20 control points and forms a cylindrical shell with a small thickness. The control points are indicated by red squares and open blue squares. Since the shell thickness is small, the control points for the inner and outer layer are partially overlapping. The quadrature points are indicated by black dots.

| Computed tri-variate NURBS aortic heart valve in the open position | | |
|--|---------|---|
| Control Point Coordinates | Weights | Knots |
| (6.495, 11.2497, 0) | 1 | ξ-direction knot values {0 0 0 .5 .5 1 1 1} η-direction knot values {0 0 1 1} ζ-direction knot values are {0 0 1 1} |
| (12.99, 7.4998, 0) | 0.866 | |
| (12.99, 0, 0) | 1 | |
| (12.99, -7.4998, 0) | 0.866 | |
| (6.495, -11.2497, 0) | 1 | |
| (7.3303, 12.9817, 19.4376) | 1 | |
| (14.6607, 8.6545, 17.8752) | 0.866 | |
| (14.6607, 0, 17.8752) | 1 | |
| (14.6607, -8.6545, 17.8752) | 0.866 | |
| (7.3303, -12.9817, 19.4376) | 1 | |
| (6.505, 11.267, 0) | 1 | |
| (13.01, 7.5113, 0) | 0.866 | |
| (13.01, 0, 0) | 1 | |
| (13.01, -7.5113, 0) | 0.866 | |
| (6.505, -11.267, 0) | 1 | |
| (7.3401, 12.999, 19.4355) | 1 | |
| (14.6802, 8.666, 17.871) | 0.866 | |
| (14.6802, 0, 17.871) | 1 | |
| (14.6802, -8.666, 17.871) | 0.866 | |
| (7.3401, -12.999, 19.4355) | 1 | |

The methodology for animating the leaflets is shown in Figure 9. Code was written in Matlab. Existing code from [5][33] was converted to Matlab. The program, *Algo4*, was modified from [5] to include extra animation steps. The original *Algo4* assembles the NURBS. It establishes a numbering system to identify local and global shape functions, and it calculates a stiffness matrix and defines a load vector of force applied on the leaflet from the blood flow. The modified code adds a damping matrix to simulate the flow resistance, a mass matrix to simulate inertial resistance to acceleration, and boundary system constraints.

The next position of the surface point was calculated from a Newmark algorithm. To compute the new control points from the surface points. First, the surface must be parameterized to obtain a knot vector. We used a chord parameterization method. Then the control points were calculated with a least square method. The stiffness matrix was re-calculated for each time step since the shape of the surface changes. The leaflets were assumed to coapt at the center of the aorta. The program terminates when the leaflets coapted length reaches a maximum length defined by Labrosse equations [23]. The height of coapted center is 47.1 mm for input dimension that were used.

Figure 9 The methodology for animating the leaflets



8 Discussion

Lumped Parameter Model

The lumped-parameter model demonstrated dynamic closure of the valve and captured the dynamical behavior of blood pressures, volumes, and flow. The model could be used to demonstrate waveform characteristics in the aortic valve region and to provide initial settings for a more complex model.

The model requires some patient-specific timing information to generate the interpolation function. Since the model only includes part of the circulatory system, the pressure of the left ventricle's driving state variable is uncoupled from the system and has to be prescribed. The model would need to be extended to include the entire circulatory system, such as with Korakianitis [21], to be able couple the hemodynamics and valve dynamics. Korakianitis [21] model also includes the ability to consider cases with aortic stenosis and aortic regurgitation. Another limitation of the model is that $V_{0,sa}$ and $V_{0,es}$ need to be measured clinically.

The lumped-parameter model could be refined to get more accurate values of E_{es} , E_{sa} , η_{sa} , R_{sc} that are difficult measure directly. The Virag and Lulić model used ejection and acceleration times and maximum velocity ejection to valid the model and adjust parameters. This verification could be supplemented with fitting the shape of the pressure and flow waveforms to patient-specific data. The roundness, skewness, plateau slant, and area bounded by these waveforms differed with adjusted settings.

The aortic valve area could be computed to verify the model against clinical data. The aortic valve orifice area was not calculated because either the actual shape of the load-bearing surface or the maximum flow velocity needs to be known for an accurate estimate. Since blood flow measurements were not incorporated into the model, an assumption about the shape of the closing valve needs to be made. The surface is probably not a regular polygon shape, but an approximation with a regular shape would provide a fast way of estimating the minimum orifice area and location.

Isogeometric Model

The isogeometric example constructed a simulated aortic valve and advanced the motion by one time step. Future work includes animating the valve to show the shape of the load-bearing surface as it opens and closes and to identify valve opening and closing times. A comparison of the timing to actual patient data could verify the accuracy of the model.

The NURBS model could also be incorporated into a FSI model to get more accurate hemodynamic results and estimates of surface shear and fatigue failure cycles. Our model could not

generate changing forces applied on the leaflet from the flow. However, a FSI model would provide the alternating reaction between the force applied on the leaflet from the flow and the effect of the resulting motion of the leaflet back on the flow. FSI capability is currently available in commercial software with finite element models.

The isogeometric model could also include a non-linear, anisotropic material model. A non-linear hyperelastic model would more accurately follow the large deformations, especially with irregular flows. The anisotropic feature would better model how the mechanical properties differ in different directions. The valve is a composite of different layers and interposed fibers. A more refined model would take advantage of the third-parameter dimension's contribution of revealing compression and extension of the thickness.

An algorithm that accepts unordered points would be able to model complex curvature of surface shapes including folds. NURBS can have free-form shapes; therefore, it is an ideal frame for fitting a set of point clouds to patient-specific data. We used a set of ordered points whose order in the parametric space grid was known and remained fixed. To take full advantage of modeling folds and complex surface curvature, surface points should be described by a cloud of unordered points. Algorithms for cloud points have been investigated [6].

Isogeometric models can model other more geometrically complex valves. Our simulated valve was an aortic valve. The mitral valve geometry is more complex because of its anchoring chords and its position in the interior of the heart. Isogeometric geometry can more easily model basal, strut, and fan cords than finite element geometry and merge the geometry into a single model.

9 Conclusions

In conclusion, we provided two examples of models of an aortic valve. The lumped-parameter system based on a model of Virag and Lulić provided a description of blood flow dynamics, and it could show waveform characteristics. It requires low computational resources and could provide an initial estimate of physiologic parameters for a more in-depth study with a finite element or an isogeometric model. The isogeometric model captured the geometry of an aortic valve with NURBS, and it could be refined by merging it with a FSI model to compute surface shear, estimate fatigue on the valve, and demonstrate valve operating mechanisms.

10 Bibliography

- [1] Y. Aboelkassem, D. Savic, and S. G. Campbell, “Mathematical modeling of aortic valve dynamics during systole,” *Journal of Theoretical Biology*, vol. 365, pp. 280–288, Jan. 2015.
- [2] M. Bavo, G. Rocatello, F. Iannaccone, J. Degroote, J. Vierendeels, and P. Segers, “Fluid-Structure Interaction Simulation of Prosthetic Aortic Valves: Comparison between Immersed Boundary and Arbitrary Lagrangian-Eulerian Techniques for the Mesh Representation,” *PLOS ONE*, vol. 11, no. 4, p. e0154517, Apr. 2016.
- [3] Borazjani, “Fluid–structure interaction, immersed boundary–finite element method simulations of bio-prosthetic heart valves,” *Computer Methods in Applied Mechanics and Engineering*, vol. 257, pp. 103–116, Apr. 2013.
- [4] H. Y. Chen, Z. Berwick, J. Krieger, S. Chambers, F. Lurie, and G. S. Kassab, “Biomechanical comparison between mono-, bi-, and tricuspid valve architectures,” *Journal of Vascular Surgery: Venous and Lymphatic Disorders*, vol. 2, no. 2, pp. 188–193.e1, Apr. 2014.
- [5] A. Cottrell, T. J. R. Hughes, and Y. Bazilevs, *Isogeometric analysis: toward integration of CAD and FEA*. Chichester, West Sussex, U.K. ; Hoboken, NJ: Wiley, 2009.
- [6] Dan and W. Lancheng, “An algorithm of NURBS surface fitting for reverse engineering,” *The International Journal of Advanced Manufacturing Technology*, vol. 31, no. 1–2, pp. 92–97, Oct. 2006.
- [7] D. Devendran and C. S. Peskin, “An immersed boundary energy-based method for incompressible viscoelasticity,” *Journal of Computational Physics*, vol. 231, no. 14, pp. 4613–4642, May 2012.
- [8] G. E. Farin, *Curves and surfaces for CAGD: a practical guide*, 5th ed. San Francisco, CA: Morgan Kaufmann, 2001.
- [9] V. Flamini, A. DeAnda, and B. E. Griffith, “Immersed boundary–finite element model of fluid–structure interaction in the aortic root,” *Theoretical and Computational Fluid Dynamics*, vol. 30, no. 1–2, pp. 139–164, Apr. 2016.
- [10] Grousson, K.-H. Lim, H.-S. Lim, E.-T. Ooi, S. L. H. Salgues, J.-H. Yeo, and W. A. Goetz, “Ventriculo-aortic junction in human root. A geometric approach,” *Journal of Biomechanics*, vol. 40, no. 10, pp. 2167–2173, Jan. 2007.
- [11] R. Haj-Ali, G. Marom, S. Ben Zekry, M. Rosenfeld, and E. Raanani, “A general three-dimensional parametric geometry of the native aortic valve and root for biomechanical modeling,” *Journal of Biomechanics*, vol. 45, no. 14, pp. 2392–2397, Sep. 2012.

- [12] R. Halevi, A. Hamdan, G. Marom, M. Mega, E. Raanani, and R. Haj-Ali, "Progressive aortic valve calcification: Three-dimensional visualization and biomechanical analysis," *Journal of Biomechanics*, vol. 48, no. 3, pp. 489–497, Feb. 2015.
- [13] P. E. Hammer, C. A. Pacak, R. D. Howe, and P. J. del Nido, "Straightening of curved pattern of collagen fibers under load controls aortic valve shape," *Journal of Biomechanics*, vol. 47, no. 2, pp. 341–346, Jan. 2014.
- [14] A. Hasan *et al.*, "Biomechanical properties of native and tissue engineered heart valve constructs," *Journal of Biomechanics*, vol. 47, no. 9, pp. 1949–1963, Jun. 2014.
- [15] M.-C. Hsu, D. Kamensky, F. Xu, J. Kiendl, C. Wang, M. C. H. Wu, J. Mineroff, A. Reali, Y. Bazilevs, and M. S. Sacks, "Dynamic and fluid–structure interaction simulations of bioprosthetic heart valves using parametric design with T-splines and Fung-type material models," *Computational Mechanics*, vol. 55, no. 6, pp. 1211–1225, Jun. 2015.
- [16] P. A. Iaizzo, R. W. Bianco, A. J. Hill, and J. D. St. Louis, Eds., *Heart Valves*. Boston, MA: Springer US, 2013.
- [17] G. B. Kalyana Sundaram, K. R. Balakrishnan, and R. K. Kumar, "Aortic valve dynamics using a fluid structure interaction model – The physiology of opening and closing," *Journal of Biomechanics*, vol. 48, no. 10, pp. 1737–1744, Jul. 2015.
- [18] D. Kamensky, M.-C. Hsu, D. Schillinger, J. A. Evans, A. Aggarwal, Y. Bazilevs, M. S. Sacks, and T. J. R. Hughes, "An immersogeometric variational framework for fluid–structure interaction: Application to bioprosthetic heart valves," *Computer Methods in Applied Mechanics and Engineering*, vol. 284, pp. 1005–1053, Feb. 2015.
- [19] C. T. Kelley, *Solving nonlinear equations with Newton's method*. Philadelphia: Society for Industrial and Applied Mathematics, 2003.
- [20] J. Kiendl, M.-C. Hsu, M. C. H. Wu, and A. Reali, "Isogeometric Kirchhoff–Love shell formulations for general hyperelastic materials," *Computer Methods in Applied Mechanics and Engineering*, vol. 291, pp. 280–303, Jul. 2015.
- [21] T. Korakianitis and Y. Shi, "Numerical simulation of cardiovascular dynamics with healthy and diseased heart valves," *Journal of Biomechanics*, vol. 39, no. 11, pp. 1964–1982, Jan. 2006.
- [22] E. Kouhi and Y. S. Morsi, "A parametric study on mathematical formulation and geometrical construction of a stentless aortic heart valve," *Journal of Artificial Organs*, vol. 16, no. 4, pp. 425–442, Dec. 2013.

- [23] R. Labrosse, C. J. Beller, F. Robicsek, and M. J. Thubrikar, “Geometric modeling of functional trileaflet aortic valves: Development and clinical applications,” *Journal of Biomechanics*, vol. 39, no. 14, pp. 2665–2672, Jan. 2006.
- [24] T. B. Le and F. Sotiropoulos, “Fluid–structure interaction of an aortic heart valve prosthesis driven by an animated anatomic left ventricle,” *Journal of Computational Physics*, vol. 244, pp. 41–62, Jul. 2013.
- [25] W. Ma and J.-P. Kruth, “NURBS curve and surface fitting for reverse engineering,” *The International Journal of Advanced Manufacturing Technology*, vol. 14, no. 12, pp. 918–927, Dec. 1998.
- [26] X. Ma, H. Gao, B. E. Griffith, C. Berry, and X. Luo, “Image-based fluid–structure interaction model of the human mitral valve,” *Computers & Fluids*, vol. 71, pp. 417–425, Jan. 2013.
- [27] G. Marom, “Numerical Methods for Fluid–Structure Interaction Models of Aortic Valves,” *Archives of Computational Methods in Engineering*, vol. 22, no. 4, pp. 595–620, Nov. 2015.
- [28] G. Marom, H.-S. Kim, M. Rosenfeld, E. Raanani, and R. Haj-Ali, “Fully coupled fluid–structure interaction model of congenital bicuspid aortic valves: effect of asymmetry on hemodynamics,” *Medical & Biological Engineering & Computing*, vol. 51, no. 8, pp. 839–848, Aug. 2013.
- [29] Mercer, J.L., “The geometry and construction of the aortic leaflet,” *J Thorac Cardiovasc Surg*, vol. 65, no. 4, pp. 511–517, Apr. 1973.
- [30] H. Mohammadi and K. Mequanint, “Prosthetic aortic heart valves: Modeling and design,” *Medical Engineering & Physics*, vol. 33, no. 2, pp. 131–147, Mar. 2011.
- [31] S. Morganti, F. Auricchio, D. J. Benson, F. I. Gambarin, S. Hartmann, T. J. R. Hughes, and A. Reali, “Patient-specific isogeometric structural analysis of aortic valve closure,” *Computer Methods in Applied Mechanics and Engineering*, vol. 284, pp. 508–520, Feb. 2015.
- [32] D. Mozaffarian, E. J. Benjamin, A. S. Go, D. K. Arnett, M. J. Blaha, M. Cushman, S. R. Das, S. de Ferranti, J.-P. Després, H. J. Fullerton, V. J. Howard, M. D. Huffman, C. R. Isasi, M. C. Jiménez, S. E. Judd, B. M. Kissela, J. H. Lichtman, L. D. Lisabeth, S. Liu, R. H. Mackey, D. J. Magid, D. K. McGuire, E. R. Mohler, C. S. Moy, P. Muntner, M. E. Mussolino, K. Nasir, R. W. Neumar, G. Nichol, L. Palaniappan, D. K. Pandey, M. J. Reeves, C. J. Rodriguez, W. Rosamond, P. D. Sorlie, J. Stein, A. Towfighi, T. N. Turan, S. S. Virani, D. Woo, R. W. Yeh, and M. B. Turner, “Heart Disease and Stroke Statistics—2016 Update: A Report From the American Heart Association,” *Circulation*, vol. 133, no. 4, pp. e38–e360, Jan. 2016.

- [33] L. A. Piegl and W. Tiller, *The NURBS book*, 2nd ed. Berlin ; New York: Springer, 1997.
- [34] F. Saleeb, A. Kumar, and V. S. Thomas, “The important roles of tissue anisotropy and tissue-to-tissue contact on the dynamical behavior of a symmetric tri-leaflet valve during multiple cardiac pressure cycles,” *Medical Engineering & Physics*, vol. 35, no. 1, pp. 23–35, Jan. 2013.
- [35] R. G. Sauvé and D. R. Metzger, “Advances in Dynamic Relaxation Techniques for Nonlinear Finite Element Analysis,” *Journal of Pressure Vessel Technology*, vol. 117, no. 2, p. 170, 1995.
- [36] F. Sotiropoulos and X. Yang, “Immersed boundary methods for simulating fluid–structure interaction,” *Progress in Aerospace Sciences*, vol. 65, pp. 1–21, Feb. 2014.
- [37] W. M. Swanson and R. E. Clark, “Dimensions and Geometric Relationships of the Human Aortic Value as a Function of Pressure,” *Circulation Research*, vol. 35, no. 6, pp. 871–882, Dec. 1974.
- [38] B. Tepole, H. Kabaria, K.-U. Bletzinger, and E. Kuhl, “Isogeometric Kirchhoff–Love shell formulations for biological membranes,” *Computer Methods in Applied Mechanics and Engineering*, vol. 293, pp. 328–347, Aug. 2015.
- [39] Z. Virag and F. Lulić, “Modeling of aortic valve dynamics in a lumped parameter model of left ventricular–arterial coupling,” *ANNALI DELL’UNIVERSITA’ DI FERRARA*, vol. 54, no. 2, pp. 335–347, Dec. 2008.
- [40] E. Votta, T. B. Le, M. Stevanella, L. Fusini, E. G. Caiani, A. Redaelli, and F. Sotiropoulos, “Toward patient-specific simulations of cardiac valves: State-of-the-art and future directions,” *Journal of Biomechanics*, vol. 46, no. 2, pp. 217–228, Jan. 2013.
- [41] N. Watton, X. Y. Luo, X. Wang, G. M. Bernacca, P. Molloy, and D. J. Wheatley, “Dynamic modelling of prosthetic chorded mitral valves using the immersed boundary method,” *Journal of Biomechanics*, vol. 40, no. 3, pp. 613–626, Jan. 2007.
- [42] N. Watton, X. Y. Luo, M. Yin, G. M. Bernacca, and D. J. Wheatley, “Effect of ventricle motion on the dynamic behaviour of chorded mitral valves,” *Journal of Fluids and Structures*, vol. 24, no. 1, pp. 58–74, Jan. 2008.
- [43] Y. Wu and X.-C. Cai, “A fully implicit domain decomposition based ALE framework for three-dimensional fluid–structure interaction with application in blood flow computation,” *Journal of Computational Physics*, vol. 258, pp. 524–537, Feb. 2014.
- [44] “2016 Harvest2 - Executive Summary Adult Cardiac Surgery Database,” The Society of Thoracic Surgeons.